Neolignans from *Piper betle* have synergistic activity against antibiotic-resistant *Staphylococcus aureus*

Chuan-Yun Xiao[1], Zhong-Lin Sun[1], Jiao Huang[1], Rong-Sheng Li[1], Jian-Ming He[1], Simon Gibbons[2], Dian-Wen Ju[1,3], Qing Mu[1*]

[1] School of Pharmacy, Fudan University, Shanghai 201203, China

[2] School of Pharmacy, University of East Anglia, Norwich NR4 7TJ, UK

[3] Shanghai Engineering Research Center of ImmunoTherapeutics, Shanghai 201203, China

[*] **Corresponding Author**

Dr. Qing Mu

School of Pharmacy, Fudan University

Shanghai 201203, China

E-mail: muqing@fudan.edu.cn

ABSTRACT

A phytochemical investigation of an extract of the leaves of *Piper betle*, guided by a synergistic antibacterial screen, led to the isolation and structural elucidation of 10 new neolignans, Pibeneolignan A−J (**1−10**), together with 11 known compounds. The structures and absolute configurations of the new compounds were elucidated on the basis of spectroscopic data, single-crystal X-ray diffraction analysis, and experimental and calculated ECD investigations. Compounds **1** and **2** are new naturally occurring neolignan skeleton, based on the cyclohept-2-ene-l,4-dione framework. We propose that these natural products are biosynthetically formed from bicyclic [3.2.1] neolignans by oxidative cleavage and ring opening at C-1′ and C-2′. Among these compounds, **9**, **13**, **15** and **16** in combination with norfloxacin against an effluxing *S. aureus* strain (SA1199B), exhibited significant synergistic activity with fractional inhibitory concentration indices (FICIs) of 0.078, 0.156, 0.125 and 0.25 respectively. Bacterial growth curves, ethidium bromide (EtBr) efflux, and qRt-PCR were further employed to verify their synergistic antibacterial mechanism. Furthermore, computational molecular modeling suggested the binding of compounds **14-17** and **19** to the active site of the modeled structure of the NorA efflux pump, which is the main efflux pump in SA1199B.

Key words: Synergism, *Piper betle*; Neolignans; Biosynthetic pathway; Antibacterial mechanism; Molecular docking.

INTRODUCTION

Antimicrobial multidrug-resistance (MDR) is one of the most significant threats to public health. The increasing prevalence of hospital- and community-acquired infections caused by MDR bacterial pathogens has raised considerable international health-care concerns as they are associated with increased morbidity and mortality and also higher clinical costs[1].

Methicillin-resistant *Staphylococcus aureus* (MRSA) is one of the most problematic clinically-relevant pathogens due to its intrinsic virulence and ability to adapt to various environmental conditions. It is a leading cause of nosocomial resistance despite the availability of effective antimicrobials[2]. In norfloxacin-resistant *Staphylococcus aureus*, the NorA efflux pump has the capability to efflux diverse antibiotics, such as fluoroquinolones and dyes such as acridine and ethidium bromide (EtBr), and contributes to MDR in the genus *Staphylococcus*[3].

Among the currently approved antimicrobials, the last discovery of a new drug class occurred more than 30 years ago[4]. To bridge this discovery gap, various strategies have been investigated including the use of synergism to enhance the activity of an antibacterial[5]. This approach uses compounds that inhibit a bacterial resistance mechanism to an existing antibiotic, effectively increasing bacterial susceptibility to older antimicrobials and therefore reviving their clinical utility[6].

Piper betle L. is a climber belonging to the Piperaceae family, used as a traditional herbal medicine in Asian countries from time immemorial[7]. In the traditional system of Chinese medicine, the leaves of *P. betle* are used to treat detumescence and as an antipruritic, for cold coughs and rheumatic osteodynia[8]. Its bioactive compounds and extracts possess multiple pharmacologies including antibacterial, anti-fungal, antitumor, anti-allergic and anti-inflammatory activities[9-11]. Phytochemical study indicated that it contains neolignans[9], benzocyclohexane oxide derivatives[10], phenolics[11], et al. In our previous antibacterial research on MRSA, we found that several neolignans from *Piper betle* had notable synergistic antimicrobial activity[10]. In order to discover further antibacterial constituents, we carried out a phytochemical investigation on *P. betle* using synergistic antibacterial activity as a guide (Fig S1).

RESULTS AND DISCUSSION

Isolation and Structure Elucidation

The leaves of *Piper betle* were extracted with 95% aqueous ethanol (10 L) at room temperature five times. The extract was concentrated and sequentially extracted with petroleum ether, chloroform and methanol. Fractionation and purification of the petroleum ether and chloroform phases by column chromatography (CC) over MCI, silica gel, reversed-phase silica gel, Sephadex LH-20 and semi-preparative HPLC afforded ten new neolignans, named Pibeneolignan A−J (**1**−**10**). The known compound (-)-Puberulin B (**11**) was also isolated and here we report its absolute configuration for the first time. Additionally, 10 known compounds were also characterised namely, licarin A (**12**)[12], (-)-accuminatin (**13**)[13], denudatin B (**14**)[14], kadsurenone (**15**)[14], (7*R*,8*R*,1′*S*)-Δ[8′]-3,4-methylenedioxy-l′-methoxy-1′,6′-dihydro-6′-oxo-7.0.4′,8.3′-neolignan (**16**)[15], (-)-burchullin (**17**)[15], burchullin (**18**)[16], (7*S*,8*S*,l′*R*)-Δ[8′]-3,4,5′-trimethoxy-(and 3,4,5,5′-tetrameth-oxy)-1′,4′-dihydro-4′-oxo-6.0.2′,7.l′-neolignan (**19**)[17], kadsurenin E (**20**)[18] and kadsurenin (**21**)[19] (Figure 1).
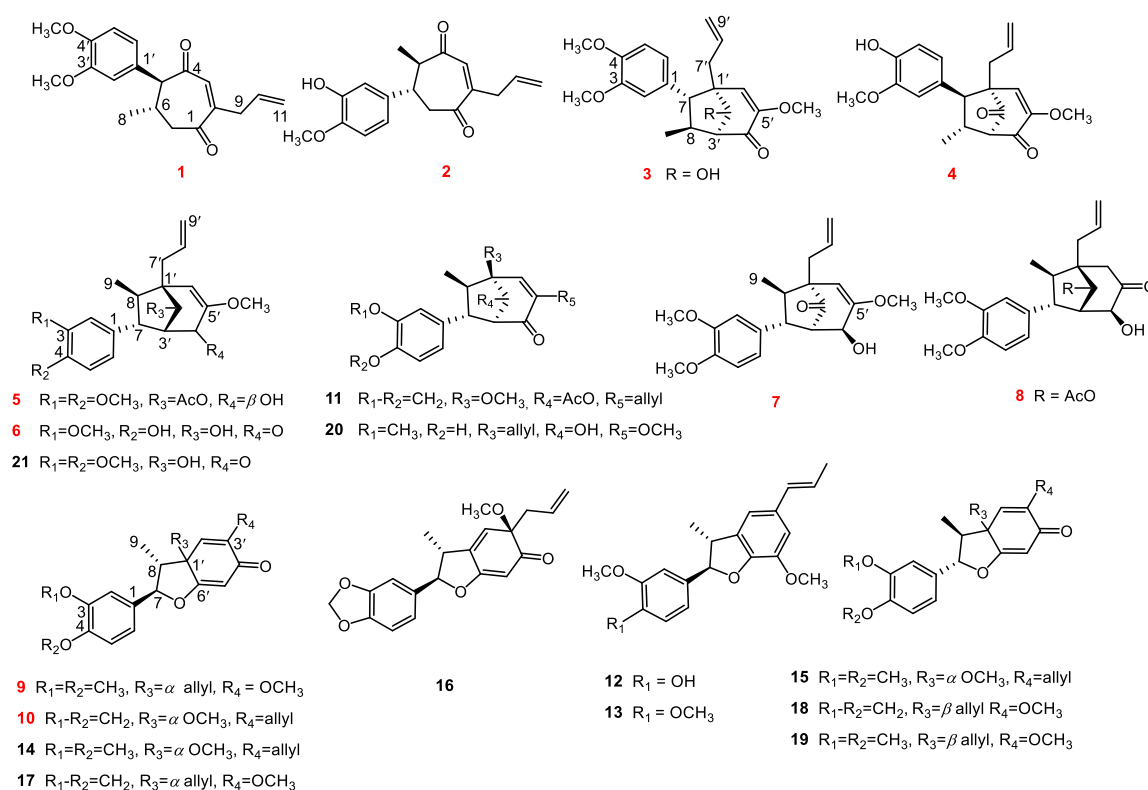

Figure 1. Structures of isolated neolignans (new compounds in red).

Pibeneolignan A (**1**) was obtained as a yellow, viscous oil. Its molecular formula was determined as $C_{19}H_{22}O_4$ with an ion at *m/z* 315.1589 (calcd. 315.1591) attributed to $[M + H]^+$ in HRESI-MS and with 9 degrees of unsaturation. Absorptions in the IR spectrum at 1748, 1689, 1501, 1488 cm^{-1} showed the presence of an α,β-unsaturated carbonyl and an aromatic moiety. The ^{1}H NMR data (in Table 1) exhibited characteristic signals for a 1,3,4-trisubstituted benzene ring: δ_H 6.74 (1H, d, 2.0 Hz, H-2′), δ_H 6.83 (1H, d, 8.4 Hz, H-5′), and δ_H 6.67 (1H, dd, 2.0, 8.4 Hz, H-6′), an olefin: δ_H 6.57 (1H, s, H-3), and an allyl group: δ_H 3.11 (1H, dd, 6.8, 16.4 Hz), 3.21 (1H, dd, 6.4, 16.0 Hz) H-9, δ_H 5.15-5.18 (2H, m, H-11), δ_H 5.82 (1H, m, H-10). The allyl group was attached to an sp^2 carbon resulting in a δ_H of 3.11 and 3.21 for H_2-9, which should it be attached to an sp^3 carbon it would resonate at $\delta_H < 2.60$ [20,21]. Further signals included those for two methoxy groups: δ_H 3.86 (3H, s, 3′-OCH$_3$), δ_H 3.87 (3H, s, 4′-OCH$_3$), a methyl group: δ_H 1.03 (3H, d, 6.4 Hz, H-8); a methylene group: δ_H 2.64 (1H, dd, 3.2, 15.2 Hz), 2.83 (1H, dd, 8.8, 15.2 Hz) H-7, and two methine groups: δ_H 2.45 (1H, m, H-5), δ_H 3.51 (1H, t, 6.4 Hz, H-6). With the aid of DEPT 135 (Figure S4) and HMQC spectra (Figure S5), the ^{13}C NMR data (Table 2) could be assigned for 19 carbon resonances, comprising three methyls (two of which were methoxy at δ_C 56.1), three methylenes (one of which was an olefinic carbon at δ_C 118.6), seven methines (five aromatic/olefinic carbons at δ_C 111.6, 111.9, 120.5, 133.9 and 146.9), and four quaternary carbons (two aromatic/olefinic carbons at δ_C 130.4 and 137.2, two oxygenated aromatic carbons at δ_C 148.8 and 149.3), two ketonic carbonyl groups (at δ_C 199.7 and 202.2). Five double bonds and two carbonyls accounted for seven degrees of unsaturation and the two remaining degrees of unsaturation indicated that compound **1** was bicyclic.

^{1}H-^{1}H COSY correlations between H-5′/H-6′, H_3-8/H-5/H-6/H_2-7, and H_2-9/H-10/H_2-11 indicated three fragments (**a**−**c**), as shown in bold bonds in Figure 2. HMBC correlations of H-2′ to C-4′/C-6′, H-5′ to C-1′/C-3′, and 3′-OCH$_3$ to C-3′, 4′-OCH$_3$ to C-4′, constructed an aromatic ring, which placed methoxy groups at C-3′ and C-4′ respectively. Further HMBC correlations between H-5 to C-3, C-4, C-6′, H_2-7 to C-1, H_3-8 to C-5, C-7, H_2-9 to C-1, C-3, furnished a 1,4-dicarbonyl seven-carbon cycle, with an aromatic ring at C-5 and an allyl group (**c**) at C-2 (Figure 2). Consequently, compound **1** possesses an unprecedented neolignan carbon skeleton, probably derived from a bicyclic [3.2.1] octane neolignan that has been opened by oxidative cleavage to a 1,4-dicarbonyl seven-carbon cycle, which has only ever been chemically

synthesised[22].

The relative configuration of **1** was established using a NOESY experiment. The presence of a correlation between H-5 and H_3-8 (Figure 2 and Figure S8) indicated that H-5 and the methyl at C-6 were on the same face. The absolute configuration of **1** was established as 5S,6S by comparison of the calculated ECD spectrum with that of the experimental one (Figure 3). Therefore, compound **1** was determined as (5S, 6S)-2-allyl-5-(3′, 4′-dimethoxyphenyl)-6-methylcyclohept-2-ene-1,4-dione.
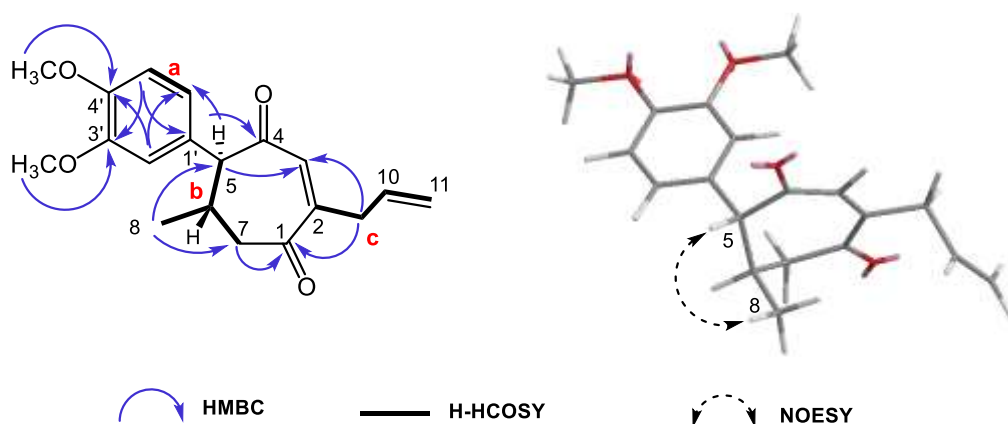

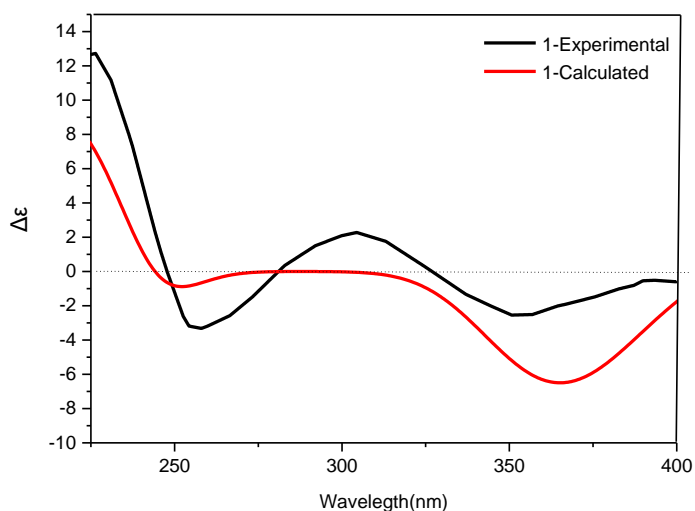Figure 2. The key HMBC (H→C), and NOESY correlations for **1**.

Figure 3. Experimental and calculated ECD spectra of **1**.

Pibeneolignan B (**2**) was obtained as a yellow viscous oil. Its molecular formula was determined as $C_{18}H_{20}O_4$, indicating 9 degrees of unsaturation and supported by an ion in the HRESI-MS at *m/z* 323.1255 (calcd. 323.1254) attributable to [M + Na]$^+$. In the IR spectrum of

2, absorption bands at 3417, 1675, 1613, 1516, 1453 cm⁻¹ showed the presence of hydroxyl, *α,β*-unsaturated carbonyl and aromatic moieties respectively. The ¹H NMR data (Table 1) were similar to those of compound **1** and indicated that **2** possesses a cyclohept-2-ene-l, 4-dione carbon skeleton. One of the major differences was that **2** had one methoxyl and a hydroxyl group rather than two methoxyls observed in **1**. HMBC correlations for **2** between H-6 to C-1/C-6′ and H₃-8 to C-4 (Figure 4) indicated that the aryl group was connected to C-6 and the methyl group was at C-5.

The relative configuration of **2** was established using a NOESY experiment. The presence of a correlation between H-6 and H₃-8 (Figure 4 and Figure S19) indicated that H-6 and Me-8 were co-facial. The absolute configuration of **2** was established 5*R*,6*S* by comparison of the calculated ECD spectrum with that of the experimental one (Figure S20). Therefore, the structure of **2** was determined as (5*R*,6*S*)-2-allyl-6-(3′-hydroxy-4′-methoxyphenyl)-5-methylcyclohept-2-ene-1,4-dione.
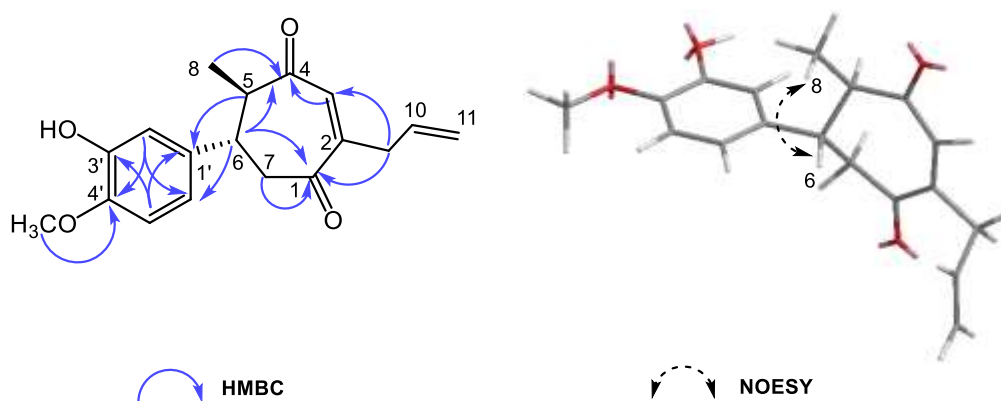

Figure 4. Key HMBC (H→C), and NOESY correlations for **2**.

Pibeneolignan C (**3**) was obtained as a colorless bulk crystal in methanol at room temperature by slow evaporation of the solvent. Its molecular formula was determined as $C_{21}H_{26}O_5$ from an ion at *m/z* 359.1853 (calcd. 359.1853) in the HRESI-MS attributable to [M + H]⁺. The IR spectrum 3481 cm⁻¹ showed absorptions for the presence of hydroxyl (3481 cm⁻¹), *α,β*-unsaturated carbonyl (1681 cm⁻¹) and an aromatic group (1609, 1514 cm⁻¹). The ¹H NMR data (Table 1) were closely similar to those of **21** (Figure 5)[19], indicating that **3** and **21** are regioisomers. In comparison with **21**, the connectivity of H-7 to C-6′ and H-9 to C-7/C-3′ by HMBC correlations in **3** indicated that the positions of the C-7 aryl group and C-8 methyl group were exchanged (Figure 5).

The cofacial-orientation between the H-7 and H_3-9 was assigned on the basis of the coupling constants ($J_{7\sim8}$ = 7.6 Hz)[24], which was supported by the degree of the dihedral angle between H-7 and H-8. Additionally, NOESY correlations between H-7 and H_3-9, H-7 and H-6′, H-2′ and H_2-7′ (Figure 6) ultimately supported the relative configuration. The ECD data (Figure S31) of **3** (negative Cotton effects at 250 nm, 325 nm) were compared with those of kadsurenin A (negative Cotton effects at 246 nm, 330 nm), whose absolute configuration was previously established by single-crystal X-ray analysis[18,25]. Consequently, the absolute configuration of **3** was established as 7*R*,8*S*,1′*S*,2′*R*,3′*S*. Finally, the structure of **3** was also unambiguously confirmed by Cu$_{K\alpha}$ X-ray crystallographic data analysis (Figure 6), and the crystal details are shown in Table S1. In summary, compound **3** was determined as (7*R*,8*S*,1′*S*,2′*R*,3′*S*)-$\Delta^{8'}$-2′-hydroxy-3,4,5′-trimethoxy-1′,2′,3′,4′-tetrahydro-4′-oxo-7.1′,8.3′-neolignan, and named Pibeneolignan C.
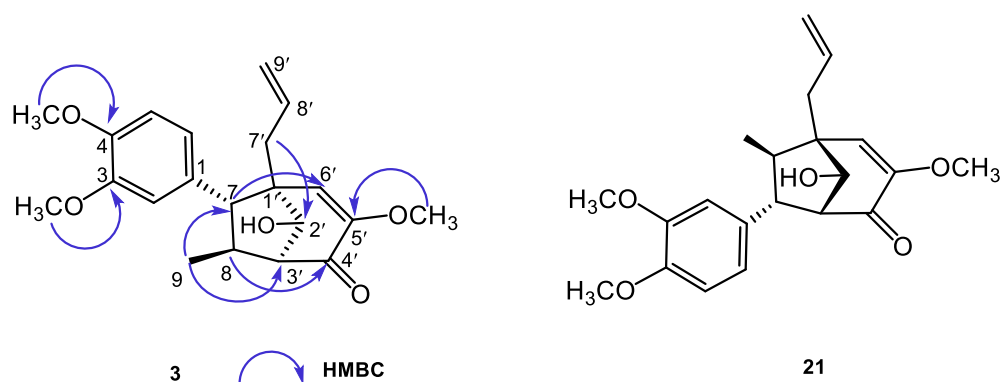

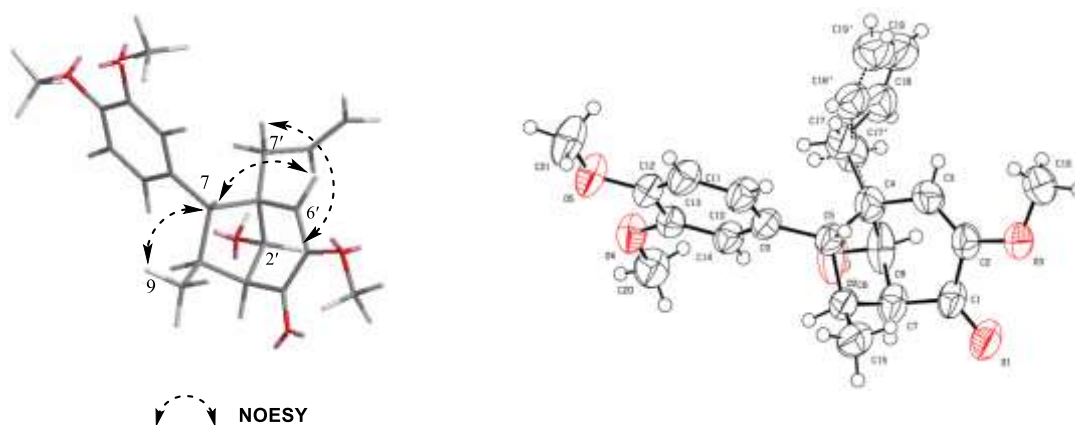Figure 5. The key HMBC (H→C) for **3** and the structure of **21**.

Figure 6. The key NOESY correlations and ORTEP drawing of **3**, Ellipsoid contour percent probability level is 50%.

Pibeneolignan D (**4**) was isolated as yellow viscous oil, and its molecular formula was

established as $C_{20}H_{22}O_5$ by an ion at m/z 343.1531 (calcd. 343.1540) ($[M + H]^+$) in the HRESI-MS. The IR spectrum showed the presence of a hydroxyl (3430 cm^{-1}), a strained ketone (1757 cm^{-1}), an α,β-unsaturated carbonyl (1689 cm^{-1}) and an aromatic moiety (1605, 1517, 1454 cm^{-1}). Comparison of the ^{1}H NMR data (Table 1) with those of **3** revealed that they were structural analogues, except for the absence of a methoxy group and an oxygenated methine in **4**. Differences in the ^{13}C NMR spectra (Table 2) of compounds **3** and **4**, suggested the presence of a carbonyl group (δ_C 203.5) in **4** and the lack of an oxygenated methine in **3** suggested oxidation at C-2′. Additionally, a hydroxyl substituent appeared in **4** at C-4 instead of a methoxy group as seen in **3**. Furthermore, the location of the hydroxyl and carbonyl group in **4** was established by HMBC correlations from H-6 to C-4, H-7 to C-2′ and H$_2$-7′ to C-2′ (Figure 7).

The NOESY correlations between H-6 and H-3′, H-7 and H$_3$-9 (Figure 7), led its relative configuration was established. The configuration of **4** was ascertained as 7*S*, 8*R*, 1′*S*, 3′*S* via comparison of the calculated and experimental ECD spectra (Figure S40). Therefore, compound **4** was determined as (7*S*,8*R*,1′*S*,3′*S*)-$\Delta^{8''}$-4-hydroxy-3,5′-dimethoxy-1′,2′,3′,4′-tetrahydro-2′,4′-dioxo-7.1′,8.3′-neolignan (Pibeneolignan D).

Pibeneolignan E (**5**) was obtained as yellow viscous oil, and its molecular formula was determined as $C_{23}H_{30}O_6$, by observation of an $[M + H]^+$ ion in the HRESI-MS at m/z 403.2099 (calcd. 403.2115). IR spectrum absorption bands at 3430, 1730, 1638, 1514, 1541, 1369 cm^{-1} showed the presence of hydroxyl, carbonyl, and aromatic moieties. The ^{1}H NMR data (Table 1) were quite similar to 7*S*,8*R*,1'*S*, 2'*S*,3'*R*,4'*S*-$\Delta^{8'}$-2'-acetoxy-3',5',3,4-tetramethoxy-4'-hydroxy-1',2',3',4'-tetrahydro-7.3',8.1'-neolignan[26], but the methoxy group in the known compound at C-3′was replaced by a hydrogen in **5** at the same position. Additionally, the planar structure of **5** was determined by the HMBC correlations as shown in Figure 7.

The relative configuration of **5** was established with a NOESY experiment, which showed correlations between H-7 and H$_3$-9, H-8 and H-4′, H-2 and H$_3$-7′, and H-2′ and H-3′/H-4′ (Figure 7). The absolute configuration of **5** was established 7*R*,8*R*,1′*R*,2′*S*,3′*S*,4′*S* by comparison of the experimental and calculated ECD spectra (Figure S48). Therefore, compound **5** was determined as (7*R*,8*R*,1′*R*,2′*S*,3′*S*,4′*S*)-$\Delta^{8''}$-2′-acetoxy-4′-hydroxy-3,4,5′-trimethoxy-1′,2′,3′,4′-tetrahydro-7.3′,8.1′-neolignan, named as Pibeneolignan E.

Pibeneolignan F (**6**) was obtained as white power. Its molecular formula was determined

Table1. The ^{1}H NMR data for compounds **1-7**

Pos	**1**[a]	**2**[a]	**3**[b]	**4**[a]	**5**[a]	**6**[b]	**7**[a]
	δ_H (*J* in Hz)	δ_H (*J* in Hz)	δ_H (*J* in Hz)	δ_H (*J* in Hz)	δ_H (*J* in Hz)	δ_H (*J* in Hz)	δ_H (*J* in Hz)
1							
2			7.21, br s	6.47, br s	6.88, br s	7.16, br s	6.63, br s
3	6.57, s	6.57, s					
4							
5	3.51, t (6.4)	2.84, m	6.78, d (8.4)	6.84, d (8.0)	6.79, d (8.4)	6.82, d (8.4)	6.68, d (8.4)
6	2.45, m	2.98, m	6.91, br d (7.8)	6.57, br d (8.4)	6.85, br d (8.4)	6.86, d (8.4)	6.78, dd (3.2, 8.8)
7	2.64, dd (3.2, 15.2) 2.83, dd (8.8, 15.2)	2.95, m 3.01, m	2.65, d (7.2)	2.69, d (6.4)	2.98, d (9.2)	2.64, d (7.2)	3.04, d (7.2)
8	1.03, d (6.4)	1.05, d (6.6)	3.00, q (7.2)	2.63, m	2.45, m	2.97, m	2.02, m
9	3.11, dd (6.8, 16.4) 3.21, dd (6.4, 16.0)	3.17, br d (6.8)	0.99, d (7.2)	1.08, d (7.2)	0.93, d (6.7)	0.99, d (7.2)	1.03, d (6.4)
10	5.82, m	5.81, m					
11	5.15-5.18, m	5.15-5.20, m					
1′							
2′	6.74, d (2.0)	6.65, br s	4.10, br s		4.93, br s	4.09, s	
3′			3.17, d (7.2)	3.73, d (6.8)	2.48, d (4.8)	3.16, d (6.6)	2.75, m
4′					4.69, br d (4.8)		4.71, br s
5′	6.83, d (8.4)	6.86, d (8.4)					
6′	6.77, dd (2.0, 8.4)	6.66, d (8.4)	6.19, s	6.21, s	4.45, s	6.18, s	4.45, s
7′			1.96, dd, (6.6, 14.4) 2.12, dd, (8.4, 14.4)	2.01, dd (7.2, 14.4) 2.21, dd (7.6, 10.4)	2.22, dd (6.0, 14.0) 2.32, dd (6.8, 15.6)	1.96, dd (6.6, 14.4) 2.12, dd (8.4, 14.4)	2.25, dd (7.6, 14.0) 2.37, dd (6.4, 16.4)
8′			5.68, m	5.64, m	5.80, m	5.68, m	5.91, m
9′			5.03-5.07, m	5.02-5.90, m	5.02-5.06, m	5.03-5.07, m	5.05-5.11, m
3-OCH$_3$			3.88, s	3.86, s	3.87, s	3.88, s	3.84, s
4-OCH$_3$			3.88, s		3.86, s		3.84, s
3′-OCH$_3$	3.86, s						
4′-OCH$_3$	3.87, s	3.89, s					
5′-OCH$_3$			3.64, s	3.69, s	3.61, s	3.64, s	3.64, s
2′-COCH$_3$					2.13, s		

[a]400 MHz for ^{1}H, [b]600 MHz for ^{1}H, **1-7** in CDCl$_3$

as $C_{20}H_{24}O_5$, involving 9 degrees of unsaturation by an ion in the HRESI-MS at *m/z* 367.1513, (calcd. 367.1516) of [M + Na]$^+$. IR spectrum absorption bands at 3443, 1679, 1610, 1514 cm^{-1} showed the presence of a hydroxyl, an *α,β*-unsaturated carbonyl and an aromatic moiety. The NMR spectroscopic data (Table 1 and Table 2) were similar to known compound **20**[18], implying

that the two compounds have the same planar structure. However, the comparison of the chiroptical data of **6** and **20** gave different ECD and optical rotations, $[\alpha]_D^{25}$: +76 (c, 0.1, CH_3OH) and $[\alpha]_D^{25}$: -75 (c, 0.1, CH_3OH) respectively. This difference indicated that the two compounds are optical isomers.

The relative configuration of **6** was further established using the NOE spectrum, which showed NOE correlations between H-7 and H_3-9 and H-8 and H-3′ (Figure 7). The absolute configuration of **6** was assigned as 7R,8R,1′R,2′S,3′R by comparison of the experimental and calculated ECD spectra (Figure S56). Finally, the structure was named Pibeneolignan F (**6**) and was determined to be (7R,8R,1′R,2′S,3′R)-$\Delta^{8'}$-4-hydroxy-3,5′- dimethoxy-1′,2′,3′,4′-tetrahydro-4′-oxo-8.1′, 7.3′-neolignan.

Pibeneolignan G (**7**) was obtained as white power. Its molecular formula was determined as $C_{21}H_{26}O_5$ with an ion at *m/z* 359.1840, (calcd. 359.1853) attributable to [M + H] $^+$ in the HRESI-MS, involving 9 degrees of unsaturation. The IR spectrum had absorption bands at 3426, 1719, 1681, 1609, 1516, 1382, 1267cm^{-1} suggesting hydroxyl, carbonyl and aromatic moieties. The ^{1}H NMR and ^{13}C NMR data (Table 1 & 2) were closely similar to those of **5**. However, the signals were different, due to the absence of an oxygenated methine in **7**. Additionally, when comparing the ^{13}C NMR spectral data (Table 2) of compounds **5** and **7**, the main difference was the presence in **7** of a strained carbonyl group (δ_C 203.5) and lack of an oxygenated methine and acetoxy group, which indicated the acetoxy group at C-2′ in **5** was replaced by carbonyl group in **7**. Furthermore, HMBC correlations (Figure 7) from H-7 to C-6/C-1′/C-2′/C-4′, H-8 to C-1/C-6′/C-7′, 3-OCH_3 to C-3, 4-OCH_3 to C-4, H-3′ to C-5′, H_2-7′ to C-2′/C-6′ further confirmed its structure.

The relative configuration of **7** was established by correlations between H-7 and H_3-9, H_3-9 and H-6′/H_2-7′ in the NOESY experiment (Figure 7). The relative configuration of C-4′ was deduced by the chemical shift of C-7 (δ_C 45.8). If the 7-aryl and 4′-OH groups are co-facial, C-7 would be affected by the γ-effect, and the chemical shift would move to a relatively low field (δ_C 56.8); Conversely, the chemical shift would move to a relatively high field (δ_C 45.8)[15,24]. The absolute configuration of **7** was therefore assigned as 7R,8R,1′S,3′R,4′S by comparing with the calculated and experimental ECD spectra (Figure S64). Finally, Pibeneolignan G (**7**) was determined as (7R,8R,1′S,3′R,4′S)-$\Delta^{8'}$-4-hydroxy- 3,4-dimethoxy-1′,2′,3′,4′-tetrahydro-2′,5′-
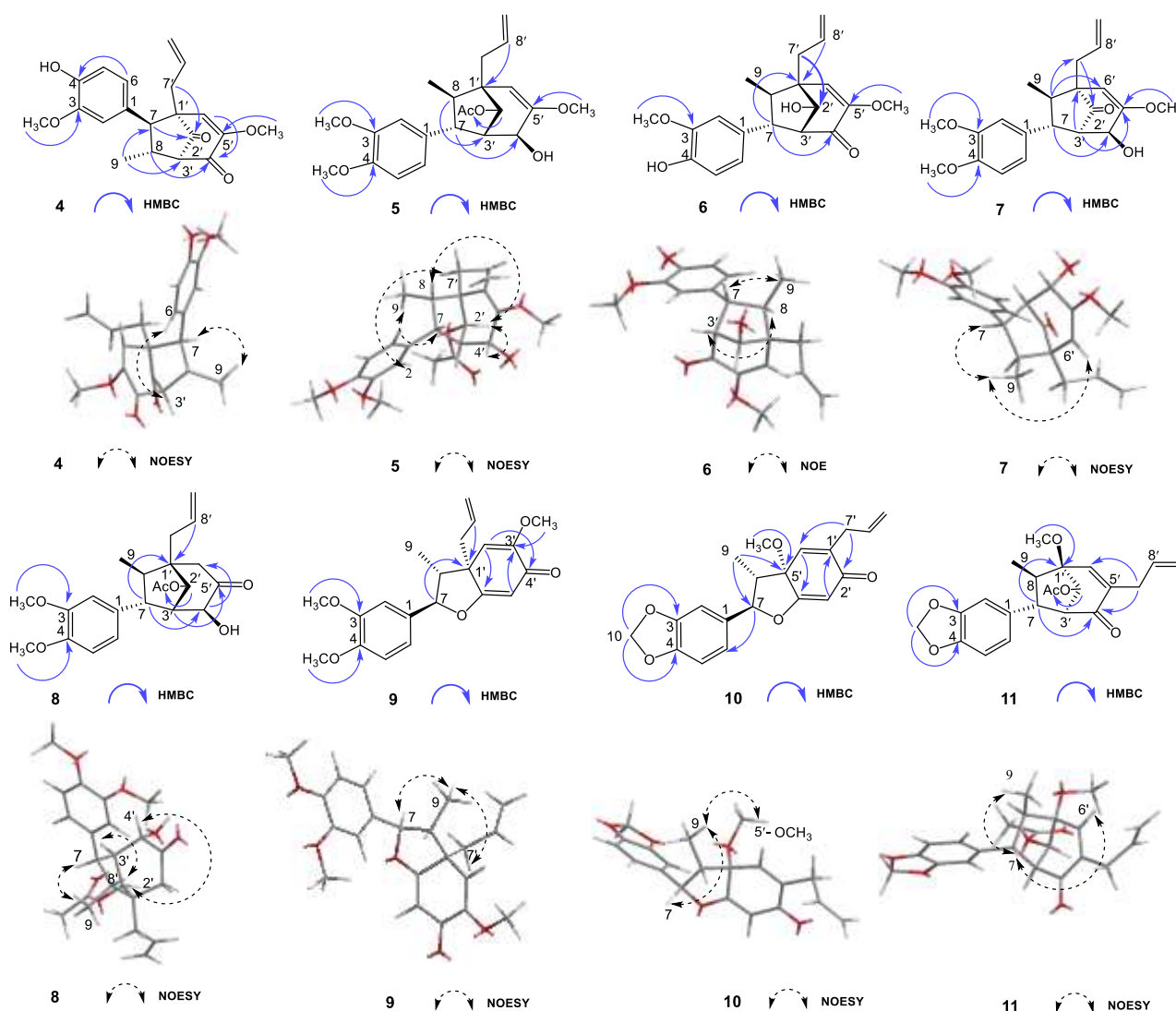
dioxo-8.1′,7.3′-neolignan.

Figure 7. The key HMBC (H→C) and NOESY or NOE correlations for **4-11**.

Pibeneolignan H (**8**) was obtained as white power, and its molecular formula was determined as $C_{22}H_{28}O_6$ with an ion at *m/z* 389.1947 (calcd. 389.1959) attributable to $[M + H]^+$ in the HRESI-MS, involving 9 degrees of unsaturation. The IR spectrum had absorption bands at 3395, 1745, 1644, 1516, 1465, 1259 cm^{-1} indicating the presence of hydroxyl, carbonyl and aromatic moieties. The ^1H NMR and ^{13}C NMR (Table 3) data for **8** were almost identical to those of 4',6'-dihydroxy-3,4-dimethoxy-3'-oxo-8.1',7.5'-neolignan-Δ:1,3,5,8'[15]. The signals were however different, due to a 2'-OH substituent of the known compound being replaced by an acetoxy substituent in **8**. Furthermore, the connectivity of the 2'-acetoxy group in **8** was established by HMBC correlations from H-2' to the carbonyl of acetoxy group and H-7 to C-2' (Figure 7).

The relative configuration of **8** was deduced by the presence of the correlations between H-7 and H-9, H-8 and H-3′, H-2′ and H-3′/4′ in NOESY experiment (Figure 7). Additionally, the chemical shift of C-7 (δ_C 43.7) indicated that H-7 and 4′-OH groups are co-facial as they are in **7**. The absolute configuration of **8** was assigned as 7R,8R,1′S,2′S,3′S,4′S by comparison of the calculated ECD spectrum with that of the experimental one (Figure S73). Finally, the structure of Pibeneolignan H (**8**) was determined to be (7R,8R,1′S,2′S,3′S,4′S)-$\Delta^{8'}$-4′- hydroxy-3,4-dimethoxy-1′,2′,3′,4′-tetrahydro-2′,5′-dioxo-8.1′, 7.3′-neolignan.

Table 2. ^{13}C NMR data for compounds **1−7** (150 MHz, **1-7** in CDCl$_3$)

Pos	1	2	3	4	5	6	7
1	199.7	199.9	133.3	132.4	137.7	132.8	137.2
2	137.2	136.6	113.7	110.5	112.1	113.0	111.0
3	146.9	148.2	148.4	146.8	148.9	146.5	149.1
4	202.2	205.2	147.9	145.2	147.4	144.6	147.7
5	67.3	42.8	110.6	114.6	111.4	113.9	111.5
6	31.7	54.7	123.0	121.9	120.1	124.0	119.5
7	49.4	50.5	62.9	58.3	49.9	63.2	45.8
8	20.1	16.9	40.8	39.1	51.1	41.0	48.5
9	35.7	36.0	16.8	18.2	12.3	16.9	12.3
10	133.9	133.7					
11	118.6	118.9					
1′	130.4	134.6	53.8	56.4	50.9	53.9	53.1
2′	111.6	109.7	80.1	203.5	80.8	80.2	210.5
3′	148.8	144.9	63.5	67.7	52.5	63.6	58.4
4′	149.3	146.9	195.5	191.4	71.8	195.6	74.3
5′	111.9	114.7	152.6	153.3	154.2	152.7	154.0
6′	120.5	120.7	128.6	123.2	99.5	128.8	98.8
7′			36.0	34.1	37.0	36.2	35.5
8′			134.7	133.4	135.1	134.8	134.2
9′			118.0	119.3	117.1	118.2	118.0
3-OCH$_3$			55.9	56.2	56.1	56.1	56.1
4-OCH$_3$			55.8		56.0		56.0
1′-OCH$_3$							
3′-OCH$_3$	56.1						
4′-OCH$_3$	56.1	56.1					
5′-OCH$_3$			55.2	55.8	55.1	55.4	55.4
2′-COCH$_3$					21.6		
2′-CO-					170.2		

Pibeneolignan I (**9**) was obtained as white power, and its molecular formula was

determined as $C_{21}H_{24}O_5$ with an ion at *m/z* 357.1692 (calcd. 357.1697) attributable to $[M + H]^+$ in the HRESI-MS, involving 10 degrees of unsaturation. The IR spectrum exhibited absorption bands at 3481, 1681, 1609, 1514 cm^{-1}, revealing the presence of hydroxyl, carbonyl, and aromatic moieties. The ^1H NMR data and ^{13}C NMR (Table 3) of **9** were identical to those of (7*S*,8*S*,l′*R*)-$\Delta^{8'}$-3,4,5′-trimethoxy-(and 3,4,5,5′-tetramethoxy)-1′,4′-dihydro-4′-oxo-6.0.2′,7.l′-neolignan[17], indicating that the two compounds have same planar structure. Additionally, comparison of the chiroptical data of **9** and the known compound gave different CD and optical rotations, $[\alpha]_D^{25}$: -47 (c, 0.1, CH_3OH) and $[\alpha]_D^{25}$: +33 (c, 0.1, CH_3OH) respectively[15,17]. This difference indicated that the two compounds are optical isomers which was further confirmed by HMBC correlations (Figure 7).

The relative configuration of **9** was established by correlations between H-7 and H_3-9 and H-9 and H_2-7′ in the NOESY experiment (Figure 7). The configuration of **9** was ascertained as 7*R*,8*R*,1′*S via* comparison of the calculated ECD spectrum with that of the experimental spectrum (Figure S81). Consequently, the structure of Pibeneolignan I (**9**) was determined to be (7*R*,8*R*,1′*S*)-$\Delta^{8'}$-3,4,5′-trimethoxy-4-oxo-7.O.2′-8.1′-neolignan.

Pibeneolignan J (**10**) was obtained as white power, and its molecular formula was determined as $C_{20}H_{20}O_5$ with an ion at *m/z* 341.1386 (calcd. 341.1384) attributable to $[M + H]^+$ in the HRESI-MS, involving 11 degrees of unsaturation. IR spectrum absorption bands at 1667, 1641, 1623, 1504 cm^{-1} indicated the presence of a conjugated carbon group and an aromatic ring. The ^1H NMR data (Table 1) were similar as in **9**, indicating that **10** was a benzofuran neolignan. Furthermore, from the comparison of these two compounds, a characteristic methylene signal of a methylenedioxy group appeared at δ_H 5.98 (2H, s)[29] in **10** instead of two methoxy groups in **9**. According to the observed HMBC correlations (Figure 7) between the protons of H-10 to C-3/C-4, H-7 to C-2/C-6, H3-9 to C-7/C-5′, H2-7′ to C-2′/C-6′, H-3′ to C-1′/C-5′ and 5′-OCH3 to C-5′ allowed the identification of the planar structure.

The relative configuration of **10** was established by correlations between H-7 and H_3-9, H_3-9 and 5′-OCH_3 in the NOESY spectrum (Figure 7), indicating that these protons are co-facial. In addition, H-8 was not subject to a 5′-OCH_3 de-shielding effect and the chemical shift of H-8 is at a relatively high field (δ_H 2.13), indicating that H-8 and 5′-OCH_3 were *trans*[27,28]. The absolute configuration of **10** was established 7*R*,8*S*,5′*R* after the comparison of the

calculated ECD spectrum with that of the experimental one (Figure S89). Finally, Pibeneolignan J (**10**) was determined to be $(7R,8S,5'R)$-$\Delta^{8'}$-5′-methyoxy-3,4-methylenedioxy-2′-oxo-7.O.4′-8.5′-neolignan.

Table 3. ^{1}H and ^{13}C NMR data of compounds **8−11**

Pos	8		9		10		11	
	δ_H (J in Hz)	δc	δ_H (J in Hz)	δc	δ_H (J in Hz)	δc	δ_H (J in Hz)	δc
1		138.4		130.2		131.4		140.1
2	6.92, br s	112.8	6.77, br s	109.3	6.79, s	106.9	6.71, br s	108.2
3		148.9		149.9		148.5		148.9
4		150.2		149.5		148.3		148.9
5	6.87, d (8.4)	113.0	6.86, br s	111.1	6.77, br s	108.4	6.84, br s	108.4
6	6.83, d (8.0)	120.5	6.87, br s	119.6	6.79, br s	121.1	6.88, br s	121.6
7	2.44, d (9.2)	43.7	5.20, d (10.2)	91.3	5.31, d (9.6)	91.5	2.40, d (8.4)	51.7
8	2.33, m	53.0	2.58, dd (7.2, 13.8)	49.6	2.13, m	50.1	2.69, m	46.8
9	0.90, d (6.4)	12.4	1.15, d (6.6)	8.6	1.12, d (6.8)	6.9	0.99, d (6.8)	13.2
10					5.98, s	101.5	5.94, s	101.2
1′		52.5		51.2		143.2		88.6
2′	5.34, s	81.3		181.7		187.2	5.30, s	75.2
3′	2.52, br s	54.5	5.82, s	102.3	5.80, s	103.0	2.96, s	60.8
4′	4.35, d (3.2)	77.8		183.1		174.7		197.6
5′		210.3		153.7		77.9		135.3
6′	2.37, m 2.62, br d (16.8)	49.4	5.43, s	108.0	6.24, s	131.2	6.71, s	146.6
7′	2.11, dd (7.6, 14.8) 2.32, m	38.2	2.30, dd (7.2, 9.0) 2.35, dd (7.2, 13.2)	36.9	3.15, m	33.7	3.02, d (7.6)	32.6
8′	5.88, m	135.3	5.56, m	131.1	5.90, m	135.3	5.83, m	134.5
9′	5.04-5.12, m	118.5	5.01, dd (1.2, 17.4) 5.07, dd (1.8, 10.2)	120.2	5.10-5.17, m	117.5	5.12-5.14, m	117.7
3-OCH$_3$	3.80, s	56.1	3.88, s	56.1				
4-OCH$_3$	3.76, s	56.2	3.89, s	56.2				
1′-OCH$_3$							3.37, s	54.1
5′-OCH$_3$			3.69, s	55.5	3.11, s	51.3		
2′-COCH$_3$	2.16, s	21.3					2.19, s	21.3
2′-CO-		170.4						169.3

400 MHz for ^{1}H NMR, 150 MHz for ^{13}C NMR; Compound **8** in acetone-D$_6$, **9-11** in CDCl$_3$

(-)-Puberulin B (**11**) was isolated as white power. Its molecular formula was determined as C$_{22}$H$_{24}$O$_6$, suggesting 11 degrees of unsaturation and with an ion in the HRESI-MS at m/z 385.1649 (calcd. 385.1646, [M + H]$^+$). IR spectrum absorption bands at 1689, 1504 and 1488

cm[-1] showed the presence of aromatic and α,β-unsaturated carbonyl moieties. The ^{1}H NMR spectroscopic data for **11** (Table 3) were identical to those of Puberulin B[20], and the HMBC and NOESY spectra (Figure 7) further identified such structure. However, the absolute configuration of Puberulin B has not been reported. The comparison of experimental and calculated ECD data (Figure S97) suggested that the absolute configuration was 7*R*,8*R*,1′*R*,2′*R*,3′*S*. Accordingly, the structure of (-)-Puberulin B was determined to be (7*R*,8*R*,1′*R*,2′*R*,3′*S*)-Δ[8′]-2′-acetoxy-1′-methoxy-3,4-methylenedioxy-1′,2′,3′,4′-tetrahydro-4′-oxo-8.1′, 7.3′-neolignan.

Proposed biosynthesis pathways of compounds 1-11

Neolignans are plant secondary metabolites originated from the shikimic acid biosynthetic pathway[29]. As outlined in Fig S101, compounds **1-11** and related compounds (**I-IX**) start from *L*-phenylalanine to afford 3,4-dihydroxypropenyl benzene and 2,4,5-trihydroxyallyl benzene, respectively. Subsequently, the bimolecular phenoxy radical 8-1′, 8-3′ and 8-5′ coupling between two different radicals will afford reactive quinones, followed by self-cyclization (7-1′, 7-3′ and 7-5′ coupling) and intramolecular dehydration condensation leading to the formation of bicyclic [3.2.1] octane neolignans (**I-III, IX**) and benzofuran neolignans (**IV, V**)[20,31]. Compounds **3**, **6** and **9** can be generated from **I, II** and **IV**, respectively, via methylation reactions. Compounds **4** and **7** were derived from **I** and **II** through methylation and oxidation. Similarly, compounds **5** and **8** were obtained by methylation, oxidation and acetylation from **II**. Additionally, compound **11** could originate from **III** via methylation, acetylation, and dehydration condensation. Compound **10** results from **V** through methylation and dehydration condensation. It is interesting to note that compounds **1** and **2** are a new structural skeleton of cyclohept-2-ene-l,4-dione neolignans and firstly rooted in **III** and **IX** via methylation. Subsequently, the adjacent hydroxyl group in bicyclic [3.2.1] octanes leads to an open cycle, which can then develop into a seven-membered cycle by oxidative cleavage[22]. Lastly, **1** and **2** were obtained by oxidation and decarboxylation[32].

Synergistic antibacterial Activities

In our previous study, neolignans from *P. betle* were revealed having potent synergistic activity in antibacterial assays against the drug-resistant *S. aureus* strain SA1199B[10]. In this

research, all compounds isolated from *P. betle* were guided by synergistic antimicrobial screening against SA1199B, but none showed direct inhibitory activity at a concentration of 256 µg/mL. Compounds **1-21** were subjected to synergistic antimicrobial assay test. The results of synergism are shown in Table 4, compounds **9**, **13**, **15, 16** reduced the minimum inhibitory concentration (MIC) values of norfloxacin against SA1199B by 16, 8, 16, 8 folds respectively, exhibiting significant synergistic activity. Compounds **1**, **5**, **12**, **14** and **17-19** showed moderate activity and reduced the MIC of norfloxacin against SA1199B 4-fold. As antibacterial combinations, compounds **1**, **5**, **9** and **12-19** with norfloxacin, showed fractional inhibitory concentration indices (FICIs) from the checkerboard assays of 0.313, 0.375, 0.078, 0.258, 0.156, 0.281, 0.125, 0.25, 0.5, 0.375, 0.5 respectively.

Table 4. Synergistic antibacterial activities of compounds **1**, **5**, **9** and **12-19** with norfloxacin.

Strains	MIC (µg/mL)					
	Compd	Compd Alone	Nor [a] Alone	Compd Combined	Nor [a] Combined	FICI
	1	256	32	16	8	0.313
	5	256	32	32	8	0.375
	9	256	32	4	2	0.078
	12	256	32	2	8	0.258
MRSA SA1199B	**13**	256	64	8	8	0.156
	14	256	32	8	8	0.281
	15	256	32	16	2	0.125
	16	256	32	32	4	0.25
	17	256	32	64	8	0.5
	18	256	32	32	8	0.375
	19	256	32	64	8	0.5

FICI ≤0.5 show synergistic effect; 0.5<FICI ≤ 1 show additive effect; 1<FICI≤ 2 show indifferent effect; 2<FICI ≤ 4 show antagonistic effect. Nor [a] = Norfloxacin. The purity of those active compounds is shown in the Fig S105-S115.

Growth curves

A growth curve assay was conducted to study the proliferation and death of *S. aureus* strain SA1199B under the influence of active compounds (**5**, **12-19**). As depicted in Fig 8, active compounds (**14，15**, @ 1/4 MIC) inhibited the growth of the bacteria when in combination with norfloxacin (8 µg/mL, 1/4 MIC) more effectively than the strain growth with norfloxacin or the compounds alone, and active compounds **5**, **12**, **13**, **18-19** were also shown similar trends (Fig S102).
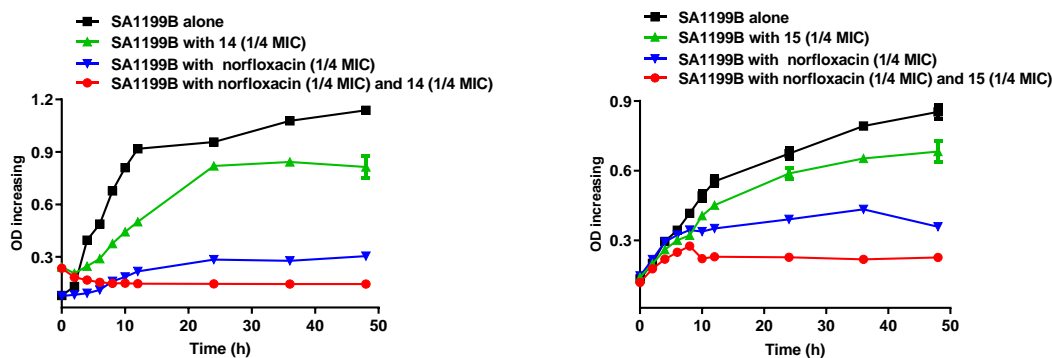
Fig 8. Growth curve assays of SA1199B in the absence or presence of norfloxacin and compounds **14** and **15**.

Inhibition of Ethidium Bromide efflux (EtBr) assays

SA1199B is a norfloxacin-resistant strain and overexpresses the *norA* gene encoding the NorA MDR efflux pump[3]. Compounds demonstrating synergistic activity (**5**, **12**, **14-19**) were tested for inhibition of EtBr efflux using a fluorometric method. As depicted in Fig 9, synergistically active compound **14** exhibited a strong inhibitory effect on EtBr efflux in SA1199B and was more active than the positive control carbonyl cyanide 3-chlorophenylhydrazone (CCCP). Compound **19** also exhibited efflux pump inhibition but was not synergistically antibacterial.
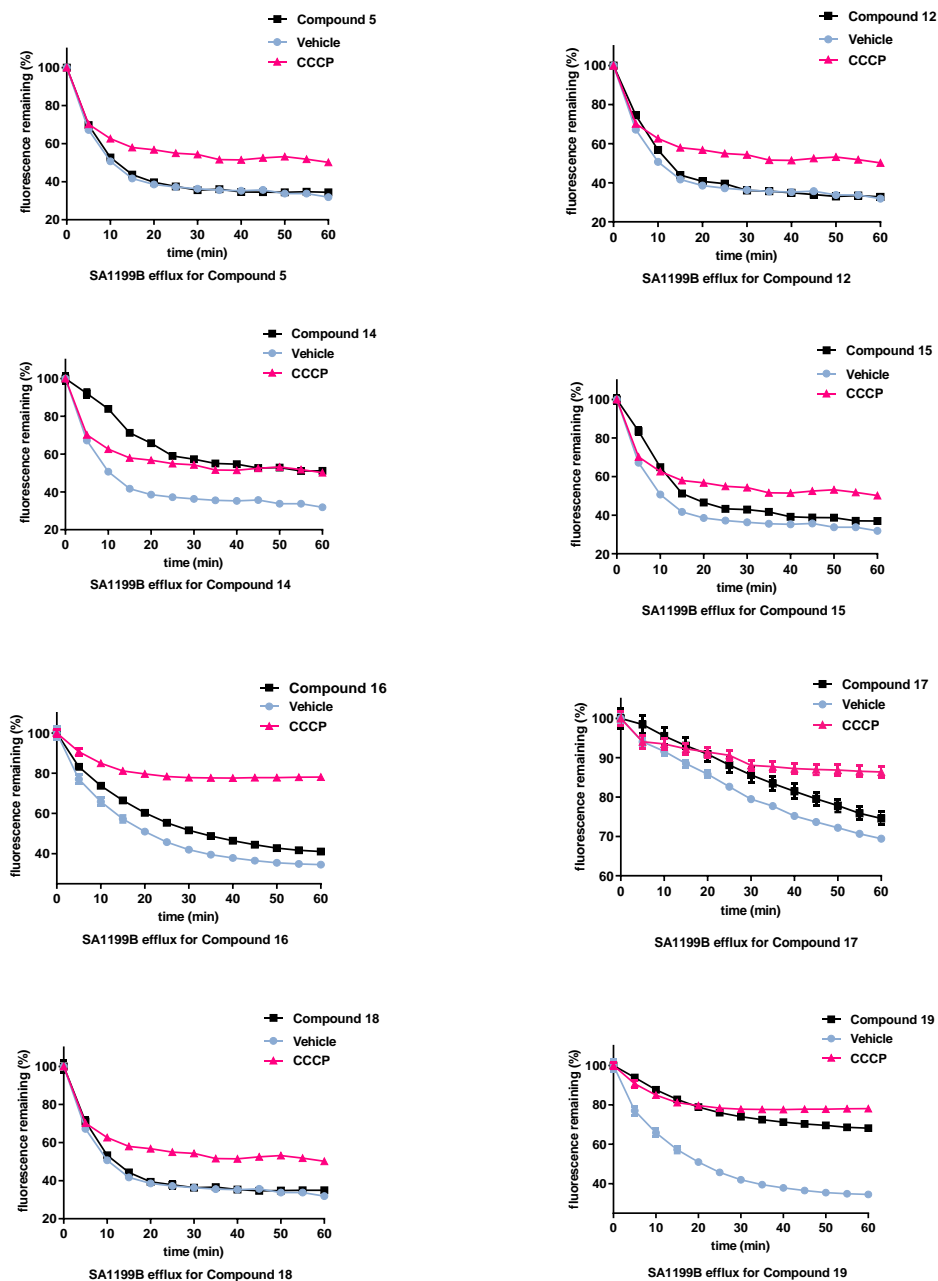
Fig 9. EtBr efflux inhibitory effects of compound **5**, **12** and **14-19** against *S. aureus* SA1199B.

qRT-PCR

To further explore how the active compounds affect the efflux system of SA1199B, the relative expression of mRNA corresponding to the *norA* gene was determined by real time qRT-PCR as compared to the drug-free condition (Fig 10). Compared with the blank control group, expression of the *norA* gene mRNA of SA1199B increased by four times with norfloxacin (8 µg/mL, 1/4 MIC) alone. This increase in expression was significantly down-regulated by the

synergistic compound **14**. Down-regulation also emerged when synergistic compounds **15-17** and **19** (FICI < 0.5) were employed in combination with norfloxacin respectively. These results indicated that synergistic effects of the compounds could be affected by the expression or decrease of the antibiotic-resistance gene *norA*.
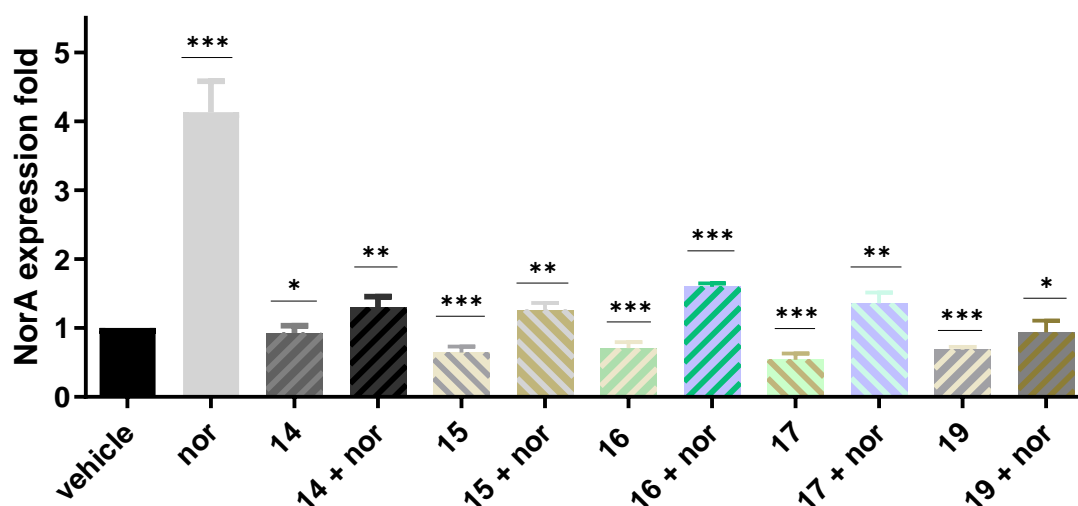

Fig 10. The effect of compounds **14-17** and **19** on mRNA expression of the *norA* gene (Data were presented as mean $\pm$ SD. n = from 3 in each group. *$P < 0.05$, **$P < 0.01$, ***$P < 0.001$.)

Cytotoxicity evaluation

Compound **14**, **15**, **18** and **19** were evaluated for their vitro cytotoxicity. Amongst them, **15** and **18** had an IC_{50} of 256 µg/mL for HEK293T cells, **14**, **19** had an IC_{50} of 128 µg/mL, and **14**, **15**, **18**, **19** had negligible cytotoxicity at the synergetic effective concentration (64 µg/mL) (Figure S102).

Molecular docking

Molecular docking between active compounds **14-17** and **19** and the NorA protein were performed to investigate their interaction. As shown in Fig 11, the binding of these compounds to amino acids predominantly involved hydrogen bond interactions along with pi-alkyl, van der Waals and carbon-hydrogen bond interactions in the predicted binding site of NorA. The details of these bindings are shown in Figure S103.
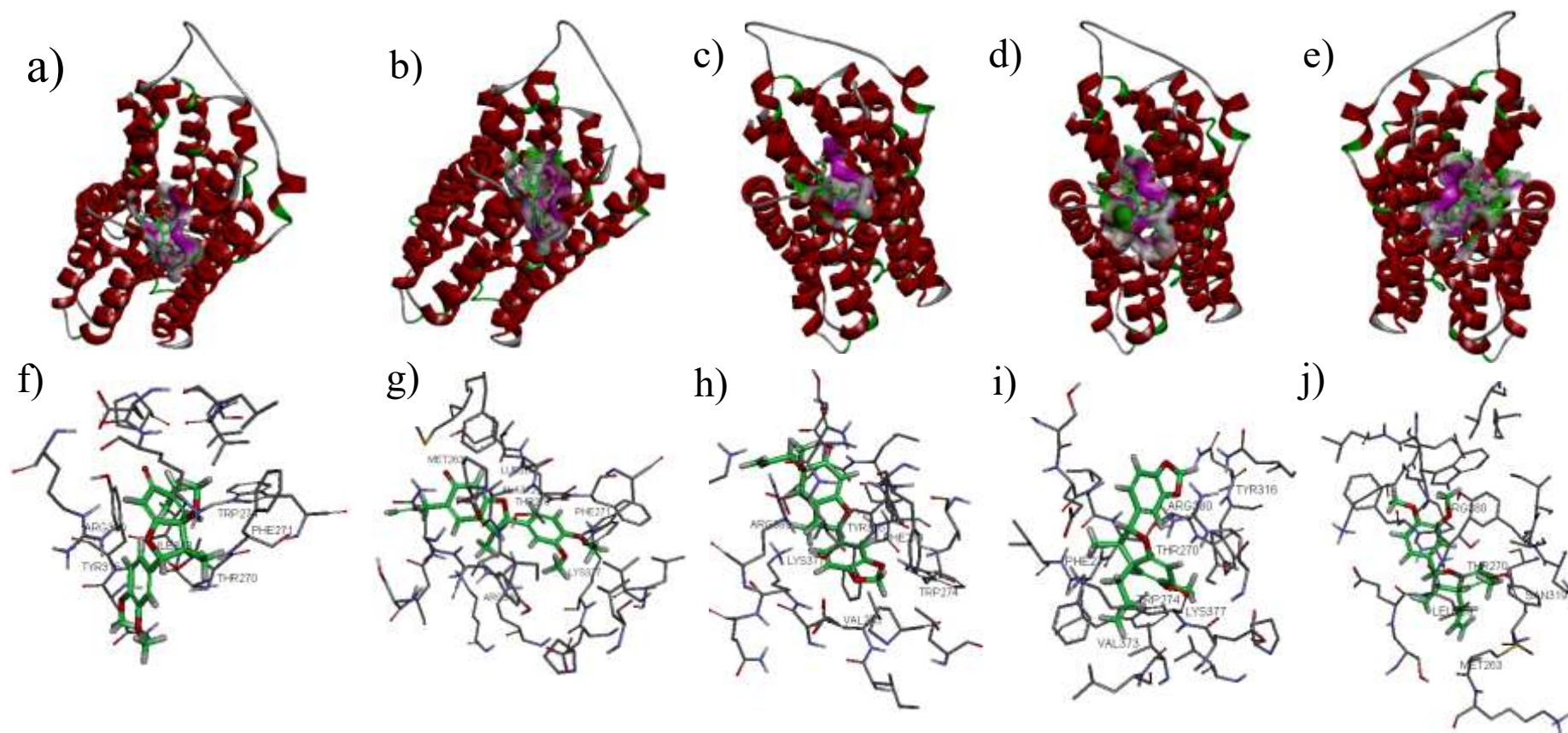
Fig 11. The molecular docking of compounds **14-17**, **19** with the NorA protein. Fig 29 a), b), c), d), e) overall structure of NorA obtained through homology modeling, with the position of **14-17** and **19**, respectively, inside the active site. Fig 29 f) **14** interacts with the closer residues ARG380, THR270, PHE271, TRP274, TYR316, ILE313; Fig 29g) **15** interacts with the closer residues THR270, LEU269, ARG380, LYS377, ALA312, MET263; Fig 29h) **16** is interacting with the closer residues TYR316, LYS377, ARG380, PHE271, VAL373, TRP274; Fig 29i) **17** interacts with the closer residues THR270, TRY316, TRP274, PHE270, ARG380, LYS377, ALA312, MET263, VAL371; Fig 29j) **19** interacts with the closer residues THR270, LEU269, ARG380, ASN319, MET263.

EXPERIMENTAL SECTION

General Experimental Procedures

Optical rotations ($[\alpha]_D$) were measured on an Autopol IV automatically at 22°C. Electronic circular dichroism (ECD) spectra for the neolignans were acquired using a JASCO-810 polarimeter (Jasco Corp., Japan) at room temperature. X-ray crystallographic data were obtained on a Bruker Apex Duo diffractometer (Cu Kα). The UV and infrared (IR) spectral data were obtained on U-2900 UV-VIS spectrophotometer (Hitachi Co. Ltd., Japan) and an iS 5 infrared spectrophotometer (Nicolet Co. Ltd., USA), respectively. 1D and 2D NMR spectra ([1]H 600 MHz and [13]C 150 MHz) were recorded on a Bruker ASCEND and ^{1}H NMR (400 MHz) were obtained on Varian Mercury Plus and the spectra were processed with MestReNova NMR (Mestrelab Research) software. Structural assignments were made with additional information from gCOSY, gHSQC, gNOESY and gHMBC experiments. HR-ESI-MS were measured on an Agilent 5973N MSD mass spectrometer. High-performance liquid chromatography (Agilent 1200, USA) was used to monitor the separated fractions and purity compounds. Optical fluorescence and density were performed using a Tecan Infinite M 1000 Pro Plate Reader (Tecan Co. Ltd., Switzerland) and a Multiskan FC (Thermo Co. Ltd., USA), respectively. During the process of separating compounds, TLC (silica gel plate HGF254, Yantai Huangwu Chemical Plant, China) was used to monitor the separation results and the purity of compounds. The silica gel (100–400 mesh, Qingdao Marine Chemical Co. Ltd., Qingdao, China) used in column chromatography was purchased from Qingdao. ODS (40−60 μm, FuJi, Silysia Chemical Ltd., Japan), and Sephadex LH-20 (Amersham Pharmacia Biotech Co. Ltd., Tokyo, Japan) were also used to isolate and purify compounds.

Plant Material

Leaves of *P. betle* were collected and identified by Professor Xu You-Kai (Xishuangbanna Botanic Garden in Yunnan Province), in December 2002, in Mengla County, Yunnan Province of China. A voucher specimen (148888) has been deposited at the Herbarium. The sample was also stored at our lab (School of Pharmacy, Fudan University).

Extraction and Isolation

The air-dried leaves of *P. betle* (4.5 Kg) were extracted by 95% ethanol (10L) at room temperature by maceration, and then filtered. This procedure was repeated five times for exhaustive extraction and combined filtrates were evaporated to a small volume, affording 406 g crude extract, which was leached by petroleum ether, $CHCl_3$, and MeOH to provide 120 g, 80 g, 140 g of extracts, respectively. The petroleum ether phase (120 g), was exhaustively extracted with 80% MeOH and ultimately yielded 22 g of a medium polar fraction. Subsequently, the 80% MeOH fraction (22 g) and part of the $CHCl_3$ fraction (10 g) were respectively subjected to microporous resin eluted with MeOH, to discard unwanted chlorophyll, and finally to afford extract A (20 g) and extract B (7.5 g) respectively. Extract A was purified through column chromatography (CC) on silica gel by the solvent system petroleum ether/EtOAc and eluted with 100:0 to 50:50, affording 13 fractions (FA-1−FA-13). The purification of FA-5 (1.0444 g) through a silica gel column eluted with petroleum ether/EtOAc (98:2) obtained compounds **12** (8.6 mg), **13** (8.5 mg) and **14** (172.0 mg). FA-6 (544.5 mg) was chromatographed on a silica gel column and eluted with petroleum ether/EtOAc (98:2) to yield compound **15** (223 mg) and fraction FA-6.2 (10 mg). Subsequently, FA-6.2 was purified by a semi-preparative HPLC column (MeOH/H_2O = 70:30) to afford compound **2** (2.0 mg, t_R = 5.5 min). FA-10 (633.1 mg) was applied to CC on ODS with a step gradient of MeOH/H_2O (70:30 to 65:35) to obtain FA-10.1−FA-10.4. FA-10.1 (21.1 mg) was chromatographed on a Sephadex LH-20 column and eluted with MeOH to afford two subfractions (FA-10.1.1-FA-10.1.2), FA-10.1.2 was purified by ODS eluting with MeOH/H_2O (65:35) to afford compound **4** (2.0 mg). FA-12 was separated on ODS eluting with MeOH/H_2O (65:35) to obtain FA-12.1−FA-12.4, and FA-12.3 was further separated by semi-preparative HPLC column (MeOH/H_2O = 60:40), to afford compound **5** (9.3 mg, t_R = 12.0 min) and compound **7** (2.0 mg, t_R = 8.2 min). FA-13 was purified by silica gel CC eluted with a step gradient elution of petroleum ether/EtOAc (90:10 to 80:20) to obtain subfractions FA-13.1-FA-13.4. FA-13.4 was further purified by ODS and semi-preparative HPLC (MeOH/H_2O = 60:40) to give compounds **8** (2.0 mg, t_R = 5.5 min) and **9** (2.0 mg, t_R = 4.5 min). Compound **18** (20.0 mg) was afforded from FA-13.1 by separation on ODS CC with a step gradient elution of

MeOH/H₂O (60:40 to 50:50). The extracts B was purified by silica gel CC with a step gradient elution of petroleum ether/acetone (100:0 to 70:30) to afford 10 fractions (FB-1−FB-10). FB-2 (17.0 mg) was applied to silica gel CC (petroleum ether/EtOAc = 95:5) to obtain compounds **10** (2.0 mg) and compounds **1** (5.0 mg). FB-3 was chromatographed on a silica gel column and eluted with a step gradient elution of petroleum ether/EtOAc (90:10 to 85:15) and further purified by Sephadex LH-20 column (chloroform/MeOH = 1:1) to afford compound **11** (9.0 mg). FB-6 was subjected to silica gel CC eluted with chloroform to give subfraction FB-6.1 and FB-6.2, and FB-6.2 was further separated using silica gel CC (petroleum ether/EtOAc = 70:30 and chloroform/EtOAc = 95:5 to 90:10) and Sephadex LH-20 (chloroform/ MeOH = 1:1). Finally, compound **16** (40.0 mg) was obtained. FB-8 was performed on CC over silica gel with a step gradient elution of chloroform/EtOAc (95:15 to 90: 10) and further purified by ODS CC (MeOH/H₂O = 60:40) to yield compounds **3** (15.0 mg) and **17** (120.0 mg). FB-9 was subjected to CC over silica gel with a step gradient elution of chloroform/MeOH (98:2 to 90:10) to yield four subfractions (FB-9.1−FB-9.4). The subfractions FB-9.1 eluted with petroleum ether/EtOAc (80:20) and chloroform/EtOAc (90:10) on the silica gel CC and chloroform/MeOH (1:1) on Sephadex LH-20 CC to give compound **19** (29.0 mg) and compound **21** (15.0 mg). Meanwhile, compound **7** (14.0 mg) and **20** (6.0 mg) were isolated from the subfraction FB-9.3 by Sephadex LH-20 and ODS CC eluted with chloroform/MeOH (1:1) and MeOH/H₂O (60:40), respectively.

Pibeneolignan A (**1**): yellow, viscous oil; HRESIMS (ESI-TOF) *m/z*: [M+H]⁺ calcd for $C_{19}H_{23}O_4$, 315.1591; Found 315.1589; UV (CH₃OH) λ_{max} (logε): 204 (2.84), 230 (2.71), 276 (2.35); IR (KBr film) ν_{max} 1748, 1689, 1501, 1488 cm⁻¹; $[\alpha]_D^{25}$: -65 (c, 0.1, CH₃OH); ECD (c, 4.5×10⁻⁴ mol/L, CH₃OH) λ_{max} (Δε) 225 (12.62), 258 (-3.33), 302 (2.23), 352 (-2.53) ; ¹H NMR data in Table 1, ¹³C NMR data in Table 2.

Pibeneolignan B (**2**): yellow, viscous oil; HRESIMS (ESI-TOF) *m/z*: [M+Na]⁺ calcd for $C_{18}H_{20}O_4Na$, 323.1254; Found 323.1255; UV (CH₃OH) λ_{max} (logε): 204 (3.49), 230 (3.29), 276 (2.88); IR (KBr film) ν_{max} 3417, 2916, 1675, 1613, 1516, 1453, 1232 cm⁻¹; $[\alpha]_D^{25}$: +20 (c, 0.1, CH₃OH); ECD (c, 3.2×10⁻⁴ mol/L, CH₃OH) λ_{max} (Δε) 257 (-0.53), 290 (0.47), 343 (-0.56) ; ¹H NMR data in Table 1, ¹³C NMR data in Table 2.

Pibeneolignan C (**3**): colorless acicular crystal; HRESIMS (ESI-TOF) *m/z*: [M+H]⁺ calcd for $C_{21}H_{27}O_5$, 359.1853; Found 359.1853; UV (CH₃OH) λ_{max} (logε): 204 (3.48), 230 (3.00),

274 (2.85); IR (KBr film) ν_{max} 3481, 2955, 1681, 1609, 1514, 1519, 1463, 1219 cm^{-1}; $[\alpha]_D^{25}$: +132 (c, 0.1, CH$_3$OH); ECD (c, 2.8×10^{-4} mol/L, CH$_3$OH) λ_{max} ($\Delta\epsilon$) 225 (2.23), 246 (-2.20), 280 (3.42), 330 (-1.15) ; ^{1}H NMR data in Table 1,^{13}C NMR data in Table 2.

Pibeneolignan D (**4**): yellow, viscous oil; HRESIMS (ESI-TOF) *m/z*: [M+H]$^+$ calcd for C$_{20}$H$_{23}$O$_5$, 343.1540; Found 343.1531; UV (CH$_3$OH) λ_{max} (logϵ): 225 (2.98), 278 (2.83); IR (KBr film) ν_{max} 3430, 2960, 1757, 1689, 1605, 1517, 1454, 1370, 1236 cm^{-1}; $[\alpha]_D^{25}$: -62 (c, 0.1, CH$_3$OH); ECD (c, 6.8×10^{-4} mol/L, CH$_3$OH) λ_{max} ($\Delta\epsilon$) 220 (8.60), 260 (−2.71), 279 (5.40), 294(-2.22), 303 (2.43), 330 (−12.18) nm; ^{1}H NMR data in Table 1, ^{13}C NMR data in Table 2.

Pibeneolignan E (**5**): yellow, viscous oil; HRESIMS (ESI-TOF) *m/z*: [M+H]$^+$ calcd for C$_{23}$H$_{31}$O$_6$, 403.2115; Found 403.2099; UV (CH$_3$OH) λ_{max} (logϵ): 204 (3.27), 223 (3.01), 276 (2.44); IR (KBr film) ν_{max} 3440, 2925, 1730, 1638, 1514, 1519, 1451, 1236 cm^{-1}; $[\alpha]_D^{25}$: +32 (c, 0.1, CH$_3$OH); ECD (c, 5.4×10^{-4} mol/L, CH$_3$OH) λ_{max} ($\Delta\epsilon$) 257 (0.95), 280 (1.90), 312 (0.49); ^{1}H NMR data in Table 1, ^{13}C NMR data in Table 2.

Pibeneolignan F (**6**): white power; HRESIMS (ESI-TOF) *m/z*: [M+Na]$^+$ calcd for C$_{20}$H$_{24}$O$_5$Na, 367.1516; Found 367.1513; UV (CH$_3$OH) λ_{max} (logϵ): 206 (3.32), 228 (3.06), 276 (2.91); IR (KBr film) ν_{max} 3443, 2926, 1679, 1610, 1514, 1453, 1272 cm^{-1}; $[\alpha]_D^{25}$: +76 (c, 0.1, CH$_3$OH); CD (c, 8.7×10^{-4} mol/L, CH$_3$OH) λ_{max} ($\Delta\epsilon$) 225 (10.01), 250 (-2.52), 275 (5.02), 312 (-3.78), 337 (1.12); ^{1}H NMR data in Table 1; ^{13}C NMR data in Table 2.

Pibeneolignan G (**7**): white power; HRESIMS (ESI-TOF) *m/z*: [M+H]$^+$ calcd for C$_{21}$H$_{27}$O$_5$, 359.1853; Found 359.1840; UV (CH$_3$OH) λ_{max} (logϵ): 205 (3.00), 225 (2.50), 276 (2.03); IR (KBr film) ν_{max} 3426, 2915, 1719, 1681, 1609, 1516, 1382, 1267 cm^{-1}; $[\alpha]_D^{25}$: -33 (c, 0.1, CH$_3$OH); ECD (c, 9.4×10^{-4} mol/L, CH$_3$OH) λ_{max} ($\Delta\epsilon$)263 (0.48), 297 (-0.02); ^{1}H NMR data in Table 1; ^{13}C NMR data in Table 2.

Pibeneolignan H (**8**): white power, HRESIMS (ESI-TOF) *m/z*: [M+H]$^+$ calcd for C$_{22}$H$_{29}$O$_6$, 389.1959; Found 389.1947; UV (CH$_3$OH) λ_{max} (logϵ): 204 (3.04), 278 (2.34); IR (KBr film) ν_{max} 3395, 2916, 1745, 1644, 1516, 1465, 1259, 1161 cm^{-1}; $[\alpha]_D^{25}$: +22 (c, 0.1, CH$_3$OH); ECD (c, 4.7×10^{-4} mol/L, CH$_3$OH) λ_{max} ($\Delta\epsilon$) 233 (-4.95), 298 (2.98); ^{1}H and ^{13}C NMR data in Table 3.

Pibeneolignan I (**9**): white power; HRESIMS (ESI-TOF) *m/z*: [M+H]$^+$ calcd for $C_{21}H_{25}O_5$, 357.1697; Found 357.1692; UV (CH$_3$OH) λ_{max} (logε): 225 (3.04), 276 (2.81); IR (KBr film) ν_{max} 3446, 2915, 1744, 1699, 1610, 1516, 1453, 1369, 1231 cm^{-1}; [α]$_D^{25}$: -47 (c, 0.1, CH$_3$OH); ECD (c, 7.8$\times$10^{-4} mol/L, CH$_3$OH) λ_{max} ($\Delta\varepsilon$) 245(-6.47), 277 (3.58), 318 (-5.16); ^{1}H and ^{13}C NMR data in Table 3.

Pibeneolignan J (**10**): white power; HRESIMS (ESI-TOF) *m/z*: [M+H]$^+$ calcd for $C_{20}H_{21}O_5$, 341.1384; Found 341.1386; UV (CHCl$_3$) λ_{max} (logε): 210 (3.68), 235 (3.01), 291 (2.63); IR (KBr film) ν_{max} 1667, 1641, 1623, 1504 cm^{-1}; [α]$_D^{25}$: -72 (c, 0.1, CH$_3$OH); CD (c, 5.9$\times$10^{-4} mol/L, CH$_3$OH) λ_{max} ($\Delta\varepsilon$) 237 (4.52), 255 (-2.75), 280 (0.89), 301 (-8.20), 350 (1.05); ^{1}H and ^{13}C NMR data in Table 3.

(-)-Puberulin B (**11**): white power; HRESIMS (ESI-TOF) *m/z*: [M+H]$^+$ calcd for $C_{22}H_{25}O_6$, 385.1646; Found 385.1649; UV (CH$_3$OH) λ_{max} (logε): 232 (3.19), 289 (2.79); IR (KBr film) ν_{max} 1748, 1689, 1504, 1488 cm^{-1}; [α]$_D^{25}$: -45 (c, 0.1, CH$_3$OH); ECD (c, 6.5$\times$10^{-4} mol/L, CH$_3$OH) λ_{max} ($\Delta\varepsilon$) 221 (10.01), 250 (-3.02), 330 (-1.56) ; ^{1}H and ^{13}C NMR data in Table 3.

Synergistic antimicrobial activity Methods

Following a protocol published earlier[10,35], hereinafter is the fractional inhibitory concentration index (FICI) according to the formula:

$$FICI = \frac{MIC(\text{antibiotic combined with compound})}{MIC(\text{antibiotic alone})} + \frac{MIC(\text{compound combined with antibiotic})}{MIC(\text{compound alone})}$$

Growth curves

Measurement of growth curves followed a protocol published earlier[10,33]with some modifications. Three groups including a norfloxacin group (8 µg/mL, 1/4 MIC) were studied. The compounds group (64 µg/mL, 1/4 MIC) and the synergism group (8 µg/mL norfloxacin and 64 µg/mL compounds, 1/4 MIC) and growth curves were determined by monitoring the optical density at 620 nm at 37°C for 2, 4, 6, 8, 10, 12, 24, 36 and 48 hours with a microwell reader. The test was repeated in triplicate.

EtBr efflux assay

Synergistic antimicrobial activity of compounds **5**, **12** and **14-19** were determined according to well-established protocols, as reported previously[34]. *Staphylococcus aureus* strain

SA1199B was inoculated in MH broth and cultured overnight (OD_{620} = 0.4), followed by the addition of CCCP (final concentrations, 100 μM) and EtBr (final concentrations, 25 μM). After incubation for 20 mins at room temperature, inocula were centrifugal at 13000g for 5 min and then re-suspended in the same volume of fresh MHB. Three groups including a vehicle group were studied, the compound group (final concentrations, 100 μM) and the CCCP group (final concentrations, 100 μM). Fluorescence of the suspension was monitored continually for one hour, once every five mins, at excitation wavelengths (530nm) and emission wavelengths (600 nm). All the tested compounds and the control were measured in triplicate.

Quantitative Real time RT-PCR (qRT-PCR) Analysis

SA1199B, an antibiotic-resistant *Staphylococcus aureus* strain, was inoculated in MH broth and cultured overnight. The bacterial suspension was then put into sterile centrifuge tubes. Drug-free MHB (blank control), norfloxacin (1/4 MIC) and compound (1/4 MIC) and the combination (1/4 MIC norfloxacin + 1/4 MIC compound) was added to each tube respectively. TRIZOL (Invitrogen) reagent was used to lyse bacteria cells and total RNA was then extracted. Subsequently, cDNA was synthesized using M-MLV (Promega) in an Applied Biosystems ViiA7 real-time PCR System (ABI) using the SYBR Premix Ex TaqTM II (TaKaRa). In these assays, the usage of primers was shown in Table S2. Under standard enzyme and cycling conditions, qRT-PCR was carried out. The relative quantity of mRNA corresponding to the NorA gene was detected by a comparative Ct or ΔΔCt method using StepOne software.

Molecular modeling

Molecular docking was performed according to the previously published paper[35].

Cytotoxicity evaluation

Cytotoxicity evaluation was performed according to the previously published paper[10].

X-ray Crystal Structure Analysis of compound 3

Compound **3** was recrystallized from methanol at 25 °C. X-ray analyses of **3** was performed on a Bruker Apex Duo diffractometer (Cu Kα) with Ga Kα radiation (λ = 1.54178 Å) at 293K. The acquisition parameters for compound **3** are provided in the Supporting Information (Table S1), and crystallographic data for **3** has been deposited at the CCDC

(deposition no. CCDC 2042889). Copies of the data can be obtained free of charge via Internet at www.ccdc.cam.ac.uk/conts/retrieving.html.

ECD Calculation Methods

The absolute configurations of **1-11** were predicted, using Gaussian 09.19 (revision A.03; Gaussian Inc.: Wallingford, CT, USA, 2016) by quantum chemical calculation. The geometries were optimized with the DFT method at the B3LYP/6-31G level of density functional theory (DFT). ECD spectra were then calculated, using the TDDFT method at the B3LYP/6-311++G** level in MeOH. Calculated ECD curves were simulated, using SpecDis (version 1.71; Berlin: Germany, 2017; http:/specdis-software.jimdo.com) with a bandwidth σ of 0.25 eV.

Supporting Information. NMR, HRMS, UV, IR, Experimental and calculated ECD spectra for compounds **1-11**, X-ray crystallographic data for compound **3**. Cytotoxic effect of **14**, **15**, **18**, **19** on HEK-293T cell line. Cartesian coordinates, the number of imaginary frequencies and computed total energies of compounds **1**, **2**, **4-11**. Growth curve assays of compounds **5**, **12-19**. Proposed biosynthesis pathways of compounds **1-11**.

ASSOCIATED CONTENT

The authors declare no competing financial interest.

References

(1) Vardakas, K. Z.; Rafailidis, P. I.; Konstantelias, A. A.; Falagas, M, E. Predictors of mortality in patients with infections due to multi-drug resistant Gram-negative bacteria: The study, the patient, the bug or the drug?, *J. Infection* 2012, 66, 401-414.

(2) Luzzaro, F.; Vigano, E. F.; Fossati, D.; Grossi, A.; Sala, A.; Sturla, C.; Saudelli, M.; Toniolo, A. Prevalence and drug susceptibility of pathogens causing bloodstream infections in northern Italy: A two-year study in 16 hospitals, *Eur J Clin Microbiol Infect Dis* 2002, 21, 849-855.

(3) Radix, S.; Jordheim, A. D.; Rocheblave, L.; N'digo, S.; Prignon, A.; Commun, C.; Michalet, S.; Dijoux-Franca, M.; Mularoni, A.; Walchshofer, N. N, N '-disubstituted cinnamamide derivatives potentiate ciprofloxacin activity against overexpressing NorA efflux pump *Staphylococcus aureus* 1199B strains, *Eur.*

J. Med. Chem 2018, 150, 900-907.

(4) Hutchings, M.; Truman, A. W.; Wilkinson, B. Antibiotics: past, present and future, *Curr Opin Microbiol* 2019, 51, 72-80.

(5) Abreu, A. C.; McBain, A. J.; Simoes, M. Plants as sources of new antimicrobials and resistance-modifying agents, *Nat. Prod. Rep* 2012, 29, 1007-1021.

(6) Ondon, B. S.; Li, S.; Zhou, Q.; Li, F. Simultaneous removal and high tolerance of norfloxacin with electricity generation in microbial fuel cell and its antibiotic resistance genes quantification, *Bioresource Tech* 2020, 304, doi: 10.1016/j.biortech.2020.122984.

(7) Madhumita, M.; Guha, P.; Nag, A. Bio-actives of betel leaf (*Piper betle* L.): A comprehensive review on extraction, isolation, characterization, and biological activity, *Phytother Res* 2020, doi: 10.1002/ptr.6715.

(8) Wu, Z. Y.; Raven, P. H. Flora of China: Volume 4, *FOC* 1999.

(9) San, T. T.; Wang, Y. H.; Hu, D. B.; Yang. J.; Zhang, D. D.; Xia, M. Y.; Yang, X. F.; Yang, Y. P. A new sesquineolignan and four new neolignans isolated from the leaves of *Piper betle*, a traditional medicinal plant in Myanmar, *Bioorg. Med. Chem. Lett* 2021, 31, doi: 10.1016/j.bmcl.2020.127682.

(10) Sun, Z. L.; He, J. M.; Wang, S Y.; Ma, R.; Khondkar, P.; Kaatz, G. W.; Gibbons, S.; Mu, Q. Benzocyclohexane oxide derivatives and neolignans from *Piper betle* inhibit efflux-related resistance in *Staphylococcus aureus*, *RSC Advances* 2016, 6, 43518-43525.

(11) Atiya, A.; Salim, M. A.; Sinha, B. N.; Ranjan Lal, U. Two new anticancer phenolic derivatives from leaves of *Piper betle* Linn., *Nat. Prod. Res* 2020, doi: 10.1080/14786419.2020.1762186.

(12) Morikawa, T.; Hachiman, I.; Ninomiya, K. Degranulation inhibitors from the arils of *Myristica fragrans* in antigen-stimulated rat basophilic leukemia cells, *J. Nat. Med* 2018, 72, 1-10.

(13) Yu, Y. U.; Kang, S. Y.; Park, H. Y.; Sung, S. H.; Lee, E. J.; Kim, S. Y.; Kim, Y. C. Antioxidant lignans from *Machilus thunbergii* protect CCl4-injured primary cultures of rat hepatocytes, *J Pharm Pharmacol* 2000, 52, 1163-1169.

(14) Ma Y.; Han G. Q.; Wang, Y. Y. PAF antagonistic benzofuran neolignans from *Piper kadsura*, *Acta Pharmacol. Sin* 1993, 25, 370-373.

(15) Ma, Y.; Han, G. Q. Benzofuranoid neolignans from *Piper kadsura*, *Zhiwu Xuebao* 1993, 35, 687-692.

(16) Cabral, M. M. O.; Mendonca, P. M.; Gomes, C. M. S.; Barbosa Filho, J. M.; Queiroz, M. M. C.; Mello, R. P. Biological activity of neolignans on the post-embryonic development of *Chrysomya megacephala*, *Fitoterapia* 2007, 78, 20-24.

(17) Filho, R. B.; Figliuolo, R.; Gottlieb, O. R. Neolignans from Nectandra species, *Phytochemistry* 1980, 19, 659-662.

(18) Han, G. Q. PAF receptor antagonistic principles from Chinses traditional durgs, *Prog Nat Sci* 1992, 3, 521-524.

(19) Ma, Y.; Han, G. Q. Neolignans from *Piper kadsuura* (II), *Chem. Pharm. Bull* 1992, 3, 635-636.

(20) Zhang, S. X.; Chen, K.; Liu, X. J.; Zhang, D. C.; Tao-Wiedmann, T. W.; Leu, S. L.; Mcphail, A. T.; Lee, K. H. The isolation and structural elucidation of three new neolignans, piperulins [corrected] A, B, and C, as platelet activating factor receptor antagonists from *Piper puberulum*, *J. Nat. Prod* 1995, 58, 540-547.

(21) Morikawa, T.; Hachiman, I.; Matsuo, K.; Nishida, E.; Ninomiya, K.; Hayakawa, T.; Yoshie, O.; Muraoka, O.; Nakayama, T. Neolignans from the Arils of *Myristica fragrans* as Potent Antagonists of CC Chemokine Receptor 3, *J. Nat. Prod* 2016, 79, 2005-2013.

(22) Rueping, M.; Kuenkel, A.; Tato, F.; Bats, J, W. Asymmetric Organocatalytic Domino Michael/Aldol Reactions: Enantioselective Synthesis of Chiral Cycloheptanones, Tetrahydrochromenones, and Polyfunctionalized Bicyclo[3.2.1]octanes, *Angew. Chem. Int. Ed* 2009, 48, 3699-3702.

(23) Rakotondraibe, L. H.; Graupner, P. R.; Xiong, Q.; Olson, M.; Wiley, J. D.; Krai, P.; Brodie, P. J.; Callmander,

M. W.; Rakotobe, E.; Ratovoson, F.; Rasamison, V. E.; Cassera, M. B.; Hahn, D. R.; Kingston, D. G, I.; Fotso, S. Neolignans and Other Metabolites from *Ocotea cymosa* from the Madagascar Rain Forest and Their Biological Activities, *J. Nat. Prod* 2015, 78, 431-440.

(24) Coy, E. D.; Cuca, L. E.; Sefkow, M. Macrophyllin-Type Bicyclo[3.2.1]octanoid Neolignans from the Leaves of *Pleurothyrium cinereum*, *J. Nat. Prod* 2009, 72, 1245-1248.

(25) Jiang, R.; Mak, T. C, W.; Fung, K. Molecular structures of two bicyclo-(3.2.1)-octanoid neolignans from *Piper kadsura*, *J. Mol. Stru* 2003, 654, 177-182.

(26) Dodson, C. D.; Stermitz, F. R.; Castro, O.; Janzen, D. H. Neolignans from Fruits of *Ocotea-Verguensis*, *Phytochemistry* 1987, 26, 2037-2040.

(27) Prasad, A. K.; Tyagi, O. D.; Wengel, J.; Boll, P. M.; Olsen, C. E.; Bisht, K. S.; Singh, A.; Sarangi, A.; Kumar, R.; Jain, S. C.; Parmar, V. S. Neolignans and A Lignan From *Piper clarkii* L, *Phytochemistry* 1995, 39, 655-658.

(28) Han, G. Q.; Li, S. M.; Li, C. L.; Springer, J. P.; Chang, M. N. Neolignans from *Piper hancei Maxim*, *Acta Pharmacol. Sin* 1986, 5, 361-365.

(29) Teponno, R. B.; Kusari, S.; Spiteller, M. Recent advances in research on lignans and neolignans, *Nat. Prod. Rep* 2016, 33, 1044-1092.

(30) Angle, S.; Turnbull, K. D. Synthesis of Neolignans via a Proposed Biosynthetic Intermediate. Total Synthesis of (A)-Futoenone, *J. Org. Chem* 1993, 58, 5360-5369.

(31) Chen, G.; Zhao, W.; Li, Y.; Zhou, D.; Ding, J.; Lin, B.; Li, W.; Yang, Y.; Liu, J.; Hou, Y.; Li, N. Bioactive chemical constituents from the seed testa of *Vernicia fordii* as potential neuroinflammatory inhibitors, *Phytochemistry* 2020, 171, doi: 10.1016/j.phytochem.2019.112233.

(32) Thongphichai, W.; Tuchinda, P.; Pohmakotr, M.; Reutrakul, V.; Akkarawongsapat, R.; Napaswad, C.; Limthongkul, J.; Jenjittikul, T.; Saithong, S. Anti-HIV-1 activities of constituents from the rhizomes of *Boesenbergia thorelii*, *Fitoterapia* 2019, 139, doi: 10.1016/j.fitote.2019.104388.

(33) Garvey, M. I.; Rahman, M. M.; Gibbons, S.; Piddock, L. J. V. Medicinal plant extracts with efflux inhibitory activity against Gram-negative bacteria, *Int J Antimicrob Agents* 2011, 37, 145-151.

(34) Lechner, D.; Gibbons, S.; Bucar, F. Plant phenolic compounds as ethidium bromide efflux inhibitors in *Mycobacterium smegmatis*, *J Antimicrob Chemother* 2008, 62, 345-348.

(35) Lan, J. E.; Li, X. J.; Zhu, X. F.; Sun, Z. L.; He, J. M.; Zloh, M.; Gibbons, S.; Mu, Q. Flavonoids from *Artemisia rupestris* and their synergistic antibacterial effects on drug-resistant *Staphylococcus aureus*, *Nat. Prod. Res* 2019, doi: 10.1080/14786419.2019.1639182.